Adhesion-Based Maximum-Seeking Brake Control for Railway Vehicles

Christoph Schwarz(✉), Tobias Posielek, and Björn Goetjes

Institute of System Dynamics and Control, German Aerospace Center (DLR), Münchener Strasse 20, 82234 Wessling, Germany
{christoph.schwarz,tobias.posielek,bjoern.goetjes}@dlr.de

Abstract. The emerging integration of mechatronic systems in modern railway vehicles enables significant improvements with respect to safety, comfort, and wear reduction. To fully exploit the potential of mechatronic systems, the German Aerospace Center (DLR) complements its validated estimation and control concepts in the field of lateral vehicle dynamics with approaches for longitudinal dynamics. The present work introduces an adhesion-based maximum-seeking brake control that offers a benefit in contrast to slip-based approaches especially in safety critical scenarios.

Keywords: Adhesion estimation · Brake control · Wheel-rail traction

1 Introduction

Besides profitability, reliability, and comfort, safety is one of the most important criteria in the decision-making of passenger transport. To ensure a safe journey, the braking process is an essential aspect for all means of transport. Regarding railway traffic, the specialty about the braking process is that the brake forces have to be transmitted via steel on steel contacts each with a size of only about $1\,\mathrm{cm}^2$. These two aspects in combination with a contamination of the wheel-rail contact can lead to highly dangerous situations where the braking distance is significantly lengthened [1].

In order to reduce the impact of poor wheel-rail conditions, an immense effort is continuously put into the improvement of braking systems and in particular the wheel slide protection system (WSP). The goal of these research activities is to minimize braking distances via a maximization of the adhesive force between wheel and rail. Some examples for sophisticated control concepts in this field are described in [2–4]. These concepts vary in their elaboration of the control algorithm but they share the same slip-based point of view. However, if slip is used as control variable, it is hard to surely reach the maximum adhesion in every single situation, since the ideal adhesion/slip ratio depends on various conditions, such as vehicle speed and track contamination, see Fig. 1.

An approach that takes this ever-changing optimum into account is presented in [5]. There, two target slip areas are defined according to the two distinct

A. Orlova and D. Cole (Eds.): IAVSD 2021, LNME, pp. 106–115, 2022.
https://doi.org/10.1007/978-3-031-07305-2_12

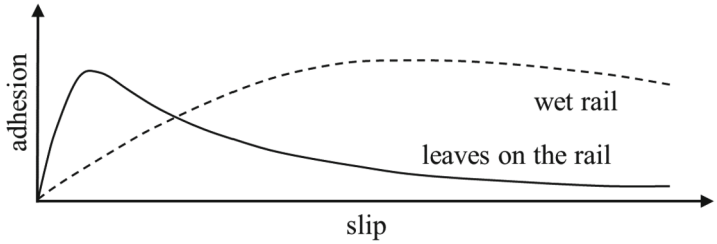

Fig. 1. Qualitative adhesion over slip behavior in case of a wet rail (dashed line) and with leaves on the rail (solid line) [5]

maxima in Fig. 1. To improve the brake performance, an algorithm continuously checks at least one wheelset in each slip area and decides what is defined as target slip area for the other wheelsets. This method is tested in track tests and allows for a significant reduction in contrast to already in-service WSP systems. In order to shorten braking distances even further, a continuously optimized brake performance in contrast to this quasi-binary approach might be the key.

In [6] a continuous PI control is combined with an adhesion estimation using swarm intelligence. However, this work focuses on traction applications and does not specifically incorporate the characteristic behavior of pneumatic brake systems, namely the binary position (open/closed) of pressure valves. In addition, the applied multi model approach might exceed the sparse computational resources of in-service train control units.

Taking a look at the automotive sector, there is a lot of research on anti-lock braking systems. However, the results cannot be directly transferred to railway vehicles, since adhesion and slip optima differ significantly.

Following from all this, the present paper introduces a numerically efficient, adhesion-based maximum-seeking brake control for critical braking scenarios with poor wheel-rail conditions. This control concept uses the adhesion information provided by a simple and generic model-based Kalman filter. First of all, the development and testing environment of the control concept is introduced in Sect. 2. Section 3 describes the synthesis of the adhesion-based control concept. Simulation results are illustrated and discussed in Sect. 4. In the end, Sect. 5 summarizes the most important contributions and gives a short outlook of the tasks to be tackled for further refinement of the control concept.

2 Development Environment for the Control Concept

The basic architecture of the control system, illustrated in Fig. 2, comprises three blocks: plant model, adhesion estimator, and controller. The controller as well as the overall framework are designed in Matlab. In this way, the single parts can directly be transferred into real-time environment, which is necessary for future prove of the control concept on test rigs.

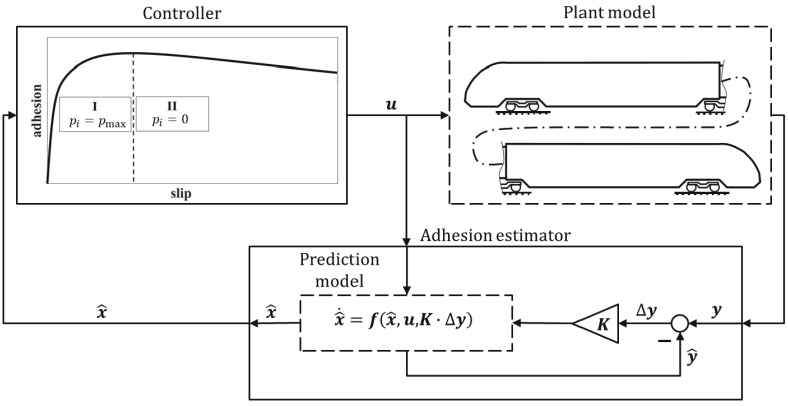

Fig. 2. Block diagram of the basic control system architecture (dashed boxes: Modelica; solid boxes: Matlab)

Plant and prediction model (dashed lines in Fig. 2) are implemented in the multi-physical and object-oriented modeling language Modelica [8]. The main advantage of Modelica in the present context is the easy and direct combination of mechanics of the brake process (force and moment equilibria) with thermal and pneumatic aspects of the friction in the brake components. The Modelica models are integrated into the development environment via the Functional Mock-up Interface (FMI), see [9].

2.1 Plant Model

As the sketch in Fig. 2 already induces, the plant model represents a two-part commuter train with a Jacobs bogie in the middle and conventional end bogies. The number of pneumatic brake units per wheelset is (from leading to trailing wheelset): 2, 1, 2, 2, 1, 2.

To reduce the numerical effort during the control synthesis, the wheelsets in the end bogies are mechanically-coupled, so there are six wheelsets but only four independent wheelset rotational velocities. Another simplification that does not hamper the validity of the braking-related behavior is the reduction to a 2-D problem in the x-z-plane, see [10]. Considering these adaptions, the state vector $\boldsymbol{x}$ of the plant model reads

$$\boldsymbol{x} = [v_x, \omega_1, ..., \omega_4, \mu_{\mathrm{b},1}, ..., \mu_{\mathrm{b},4}, \Delta z_1, ..., \Delta z_6, \Delta \dot{z}_1, ..., \Delta \dot{z}_6]^T . \tag{1}$$

The first states v_x and ω_i, with $i = 1, ..., 4$, represent the translational vehicle velocity and the rotational wheelset velocities, respectively. The corresponding system dynamics for v_x can be deduced from the longitudinal force equilibrium over the entire vehicle and for ω_i from the moment equilibria for each of the four independently rotating wheelsets. The states $\mu_{\mathrm{b},i}$ describe the friction coefficients between brake pad and brake disc. The modeling of instantaneous pad friction

behavior is still subject of research. In the present work, the approach proposed in [11] is used, which takes the thermal influences on $\mu_{\mathrm{b},i}$ into account.

The states Δz_j $(j = 1, ..., 6)$ and $\Delta \dot{z}_j$ are the deflections in the primary suspensions and their time derivatives, respectively. These twelve states are introduced to reproduce the vertical and pitch motions of the three bogies. On the contrary, the vertical and pitch motions of the two car bodies can be neglected, since spring and damper coefficients of the secondary suspension are usually much lower than of the primary suspension and, thus, the influences of the car bodies on the braking process are insignificant.

The last state-related aspect to be mentioned is the continuous modeling of the wheel-rail contact behavior. To calculate the adhesion between wheel and rail

$$\alpha_{x,i}\left(s_i, v_x\right) = \frac{F_{x,i}}{F_{z,i}}\,, \tag{2}$$

with the longitudinal contact force $F_{x,i}$, the normal contact force $F_{z,i}$, and the slip s_i, the formulation of Polach [12] is implemented in the plant model. The slip s_i is defined as

$$s_i = 1 - \frac{r_w \omega_i}{v_x} \quad \text{and} \quad \dot{s}_i = f_{s,i}\left(v_x, \alpha_{x,i}\right) + g_{s,i}\left(\mu_{\mathrm{b},i}, v_x\right) u_i\,, \tag{3}$$

where the term $g_{s,i}\left(\mu_{\mathrm{b},i}, v_x\right)$ is negative in the considered region. A more detailed description of the system dynamics $f_{s,i}$ and $g_{s,i}$ is omitted due to the limited space of this article. According to [13], the numerical efficacy of the Polach theory and its accurate modeling of the adhesion behavior for higher creepages makes it well suited in the present context.

Besides the states, the plant system is described by its inputs $\boldsymbol{u}$ and outputs $\boldsymbol{y}$. When dealing with brake control, the inputs are the brake pressures

$$\boldsymbol{u} = \left[p_1, p_2, p_3, p_4\right]^T\,, \tag{4}$$

which correspond to the four independent wheelset rotations and affect their moment equilibria but have no direct influence on the longitudinal force equilibrium of the vehicle. Combining these equilibria with the brake pad friction dynamics and the wheel-rail contact model leads to the state space formulation

$$\dot{\boldsymbol{x}} = \boldsymbol{f}\left(\boldsymbol{x}\right) + \boldsymbol{g}\left(\boldsymbol{x}\right)\boldsymbol{u} \tag{5}$$

where $\boldsymbol{f}$ and $\boldsymbol{g}$ determine the state dynamics and can be found in [14]. For this work, only the velocity dynamics $\dot{v}_x = f_v(\boldsymbol{\alpha}_x)$ which are a function of the adhesion and the slip dynamics as given in Eq. (3) are required for the proof of the controller design.

A decision on the outputs has to trade off the technical and economic effort for the sensor implementation against the reliability of the estimator. For the present application, the output configuration is defined as

$$\boldsymbol{y} = \left[v_x, \omega_1, ..., \omega_4, \Delta z_1, ..., \Delta z_6, \dot{v}_x\right]^T\,. \tag{6}$$

Compared to the current equipment of modern vehicles, only the detection of Δz_j causes additional effort. Anyhow, as shown in [14] the adhesion estimator would not necessarily need this information to get reliable estimation results.

2.2 Adhesion Estimator

Adhesion between wheel and rail is not directly measurable in regular operation due to technical and economic reasons. To provide this essential information during braking maneuvers, an estimator is designed. The applied estimator, an Extended Kalman Filter (EKF), is successfully deployed for the adhesion and brake pad friction estimation in [15].

To get the adhesion information, the coefficients $\hat{\boldsymbol{\alpha}}_x$ are integrated into the state vector $\hat{\boldsymbol{x}}$ of the estimator prediction model

$$\hat{\boldsymbol{x}} = \left[\hat{v}_x, \hat{\omega}_1, ..., \hat{\omega}_4, \hat{\mu}_{\mathrm{b},1}, ..., \hat{\mu}_{\mathrm{b},4}, \hat{\alpha}_{x,1}, ..., \hat{\alpha}_{x,4}, \Delta\hat{z}_1, ..., \Delta\hat{z}_6, \Delta\dot{\hat{z}}_1, ..., \Delta\dot{\hat{z}}_6\right]^T. \quad (7)$$

A more detailed description of the estimator design can be found in [15].

3 Brake Control Synthesis

3.1 Problem Formulation

The goal of this work is to design an adhesion-based control law that minimizes the braking distance r_x which results from the point of time t_f when v_x reaches 0 m/s. Due to monotonicity arguments, this is equivalent to maximizing the adhesion for each wheelset, i.e. we need to solve the optimization problem

$$\max_{u_i} \quad \int_0^t |\alpha_{x,i}(s_i(\tau), v_x(\tau))| \, \mathrm{d}\tau \quad (8)$$

subject to $\dot{s}_i, \dot{v}_x$ as in Eq. (3), (5) and $\dot{\mu}_{\mathrm{b},i}, \alpha_{x,i}$ according to [11,12].

The hereby considered parameter configurations lead to adhesion-slip curves similar to the ones shown in Fig. 1. They all admit a region of the slip $[0, s_{\mathrm{con}}]$ for which the adhesion is concave. This allows to design the extremum seeking control law as in the next section.

3.2 Maximum-Seeking Control Strategy

To obtain a robust solution of the optimization problem (8), we derive an appropriate sliding mode control law. The proposed control law uses only the estimated time derivatives of adhesion and slip. For the control synthesis and its stability proof the estimated values are assumed to be exact.

In the classical sliding mode sense, it is straightforward to design a maximum seeking control by defining the maximum as the equilibrium in the switching function and ensure that the resulting sliding manifold is attractive, see e.g. [17]. In this case, the desired switching function σ_i and the control law u_i take the form

$$\sigma_i = \frac{\partial \alpha_{x,i}(s_i, v_x)}{\partial s_i} \qquad u_i = L \operatorname{sgn}\left(\frac{\partial \alpha_{x,i}(s_i, v_x)}{\partial s_i}\right) \quad (9)$$

for a designed gain $L \in \mathbb{R}$. However, this control law cannot be directly implemented, because the exact description of the adhesion function $\alpha_x(\cdot)$ is not known but merely its estimated function value $\hat{\alpha}_{x,i}(s_i(t), v_x(t))$ at the current time t. Therefore, the sliding manifold needs to be formulated in a different way.

The idea to emulate this control is illustrated in the controller block in Fig. 2. We use the product of the derivatives of adhesion and slip with respect to time in the switching function

$$\bar{\sigma}_i = \dot{s}_i(\boldsymbol{\varrho}_i, u_i)\dot{\alpha}_{x,i}(\boldsymbol{\varsigma_i}) \tag{10}$$

with $\boldsymbol{\varrho}_i = (v_x, \alpha_{x,i}, \mu_{b,i})$ and $\boldsymbol{\varsigma_i} = (s_i, v_x)$, to drive the adhesion with the corresponding sliding mode control law to its maximum. Indeed, it can be shown that this control law is equivalent to the desired control law (9) and solves the control task as shown in the following theorem.

Theorem 1. *The sliding mode control law*

$$u_i = L\, sgn\left(\dot{s}_i(\boldsymbol{\varrho}_i, u_i)\dot{\alpha}_{x,i}(\boldsymbol{\varsigma_i})\right) \tag{11}$$

drives the adhesion of the system (5) to its maximum, if $L \in \mathbb{R}$ is chosen sufficiently high and the slip stays in the concave region, i.e. $s \in [0, s_{\text{con}}]$.

Proof. Using Eq. (3) for s and the Polach formulation for α_x allows to write the switching function as

$$\bar{\sigma}_i = \dot{s}_i(\boldsymbol{\varrho}_i, u_i)\left(\frac{\partial \alpha_{x,i}(\boldsymbol{\varsigma_i})}{\partial s_i}\dot{s}_i(\boldsymbol{\varrho}_i, u_i) + \frac{\partial \alpha_{x,i}(\boldsymbol{\varsigma_i})}{\partial v_x}\dot{v}_x\right) \approx \frac{\partial \alpha_{x,i}(\boldsymbol{\varsigma_i})}{\partial s_i}\dot{s}_i(\boldsymbol{\varrho}_i, u_i)^2\,. \tag{12}$$

Neglecting the second term bases upon the assumptions that the sensitivity of $\alpha_{x,i}$ with respect to s_i is much higher than with respect to v_x, see [12], and $\dot{s}_i(\boldsymbol{\varrho}_i)$ is usually higher than $\dot{v}_x$ due to the high inertia of the vehicle. This makes clear that σ_i is identical to zero if $\frac{\partial \alpha_{x,i}(\boldsymbol{\varsigma_i})}{\partial s_i} = 0$ or $\dot{s}_i(\boldsymbol{\varrho}_i) = 0$. Then we can see for $\dot{s}_i(\boldsymbol{\varrho}_i) \neq 0$ that

$$\operatorname{sgn}(\bar{\sigma}_i) \approx \operatorname{sgn}\left(\frac{\partial \alpha_{x,i}(\boldsymbol{\varsigma_i})}{\partial s_i}\dot{s}_i(\boldsymbol{\varrho}_i, u_i)^2\right) = \operatorname{sgn}\left(\frac{\partial \alpha_{x,i}(\boldsymbol{\varsigma_i})}{\partial s_i}\right) = \operatorname{sgn}(\sigma_i)\,. \tag{13}$$

We show that the system converges to $\sigma_i = 0$ by considering the Lyapunov candidate

$$V(x) = \frac{1}{2}\sigma_i^2\,. \tag{14}$$

We obtain the derivative of V with respect to time as

$$\begin{aligned}
\dot{V}(\boldsymbol{x}) &= \sigma_i\dot{\sigma}_i = \sigma_i\left(\frac{\partial^2 \alpha_{x,i}(\boldsymbol{\varsigma_i})}{\partial s_i^2}\dot{s}_i(\boldsymbol{\varrho}_i, u_i) + \frac{\partial^2 \alpha_{x,i}(\boldsymbol{\varsigma_i})}{\partial v_x \partial s_i}\dot{v}_x(\boldsymbol{x})\right) \\
&= \sigma_i\frac{\partial^2 \alpha_{x,i}(\boldsymbol{\varsigma_i})}{\partial s_i^2}\left(f_{s,i}(\boldsymbol{\varrho}_i) + g_{s,i}(\boldsymbol{\varrho}_i)u_i + \left(\frac{\partial^2 \alpha_{x,i}(\boldsymbol{\varsigma_i})}{\partial s_i^2}\right)^{-1}\frac{\partial^2 \alpha_{x,i}(\boldsymbol{\varsigma_i})}{\partial v_x \partial s_i}f_v(\boldsymbol{\alpha}_x)\right) \\
&= \frac{\partial^2 \alpha_{x,i}(\boldsymbol{\varsigma_i})}{\partial s_i^2}\left(Lg_{s,i}(\boldsymbol{\varrho}_i)\,|\sigma_i| + \phi_i(\boldsymbol{\varrho}_i, \boldsymbol{\alpha})\sigma_i\right)
\end{aligned} \tag{15}$$

with $\phi_i(\boldsymbol{\varrho}_i, \boldsymbol{\alpha}) = f_{s,i}(\boldsymbol{\varrho}_i) + \left(\frac{\partial^2 \alpha_{x,i}(\boldsymbol{\varsigma_i})}{\partial s_i^2}\right)^{-1} \frac{\partial^2 \alpha_{x,i}(\boldsymbol{\varsigma_i})}{\partial v_x \partial s_i} f_v(\boldsymbol{\alpha}_x)$. It can be seen that $\frac{\partial^2 \alpha_{x,i}(\boldsymbol{\varsigma_i})}{\partial s_i^2} < 0$ due to $\alpha_{x,i}$ being concave in the considered region. Further, the remaining terms can be dominated in the sliding mode sense using a sufficiently high L. This ensures with $g_{s,i}(\boldsymbol{\varrho}_i) < 0$ that $\dot{V}(\boldsymbol{x}) < 0$, which renders the sliding manifold attractive and the adhesion converges to its maximum value. *q.e.d.*

Note that the approximation in Eq. (12) leads to α_x not being at the exact maximum but very close to it dependent on the magnitude of the term $\frac{\partial \alpha_{x,i}(\boldsymbol{\varsigma_i})}{\partial v_i} \dot{v}_x$. Another option for the switching function $\frac{\dot{\alpha}_{x,i}}{\dot{s}_i}$ allows a similar proof for optimality, but its implementation leads to numerical issues for $\dot{s}_i$ close to zero, which is why we have chosen to use the switching function (10) instead. The choice of L depends on $g_{s,i}$ and ϕ_i and is generally subject to optimization. It might also be chosen as a function of the states to compensate their influences. However, in the present context of braking control the maximum brake pressure $p_{\max}$ is usually predefined by the dimensioning of the brake system and, thus, the adjustability of L is limited. Furthermore, it may occur that the choice of L leads to a slip value being in the non-concave part of α_x, i.e. $\frac{\partial^2 \alpha_{x,i}(\boldsymbol{\varsigma_i})}{\partial^2 s_i} > 0$ and σ is not strictly increasing in this region. Nevertheless, this does not forbid the attractiveness of $\sigma = 0$ but it requires an adaptation of the Lyapunov function.

Finally, the control law is combined with a limitation of α_x required by the operational restriction of the actual adhesion coefficient $\alpha_{x,\max} \leq 0.15$ defined in [16]. In contrast to a slip-based brake control, the presented concept offers the advantage of a strict adherence to $\alpha_{x,\max}$ facilitated by the estimated adhesion information $\hat{\alpha}_x$.

4 Presentation and Discussion of Brake Control Results

In order to test and validate the performance of the adhesion-based brake control (ABC), three test scenarios are generated, all with an initial speed of 80 km/h. They differ in their maximum wheel-rail friction coefficient μ_0 of the Polach contact formulation. Figure 3 illustrates the time-variant μ_0 with a trapezoid (top), sine sweep (middle), and random characteristic (bottom). This compilation of cases allows to validate the robust performance of the brake control in various typical brake scenarios: (i) trapezoid e.g. induced by repeated changes between shady and sunny track sections; (ii) sine sweep representing low-frequency, continuous variations of the track conditions; (iii) random case with high-frequency changes caused by a random distribution of wet leaves on the rails. The minimum μ_0 rises in all scenarios from the front (blue line) to the rear wheelset (purple line). This increase represents the well-known conditioning effect, i.e. the front wheelsets clean up the rails so that the rear wheelsets have a higher μ_0.

To allow for a meaningful assessment of ABC, a slip-based two-level controller (SBC), with $s_{low} = 10\%$ and $s_{high} = 15\%$, is applied to the test cases as reference. The achieved braking distances are listed in Table 1. The reduction of braking distances with ABC by at least 8.8% compared to SBC generally confirms the

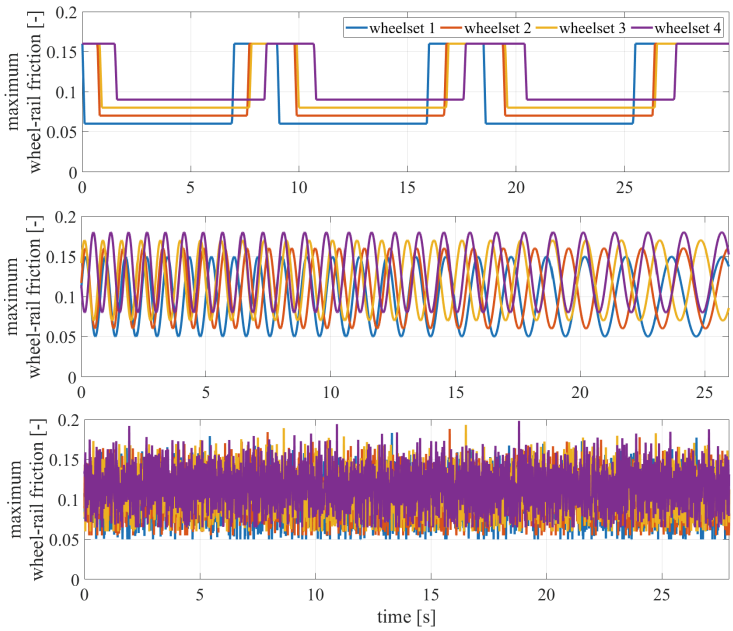

Fig. 3. Maximum wheel-rail friction coefficients in the test scenarios (from top to bottom: trapezoid, sine sweep, random scenario

Table 1. Achieved braking distances with novel ABC and state-of-the-art SBC

	Trapezoid	Sine sweep	Random
SBC	382.9 m	316.2 m	339.6 m
ABC	333.4 m (−12.9%)	286.6 m (−9.4%)	309.6 m (−8.8%)

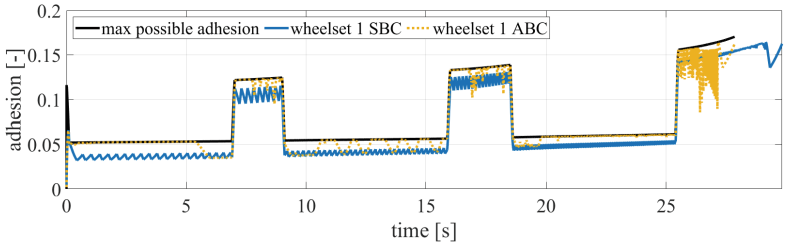

Fig. 4. Comparison of adhesion results with novel ABC and state-of-the-art SBC

functionality of the novel brake control concept. For a more detailed analysis, the adhesion results at the first wheelsets using ABC (yellow dotted line) and SBC (blue solid line) as well as the maximum achievable adhesion (black solid line) are shown in Fig. 4 for the trapezoidal test case. The results of the other wheelsets are left out at this point, since they are qualitatively similar. First of all, it can be seen that the adhesion values with SBC are considerably lower than with ABC and in consequence the braking process lasts approximately 2 s longer. Comparing ABC with the maximum achievable adhesion curve demonstrates that almost throughout the entire brake maneuver both lines are very close, so the developed concept proves its functionality. The phases with a suboptimal adhesion between $t = 9\,\mathrm{s}$ and $t = 16\,\mathrm{s}$ emerge from the dynamic coupling between the four wheelsets, which for example affect the normal contact forces $F_{z,i}$ and according to Eq. (2) also the adhesion.

In addition, the ideal performance of ABC falls off after the last rise of μ_0 at about $t = 25\,\mathrm{s}$ and a significant chattering occurs. This behavior is caused by three interacting effects: (i) for low v_x the slip is extremely sensitive to over-critical brake demands, since v_x is in the denominator of s_i; (ii) the limitation of $\alpha_{x,\max} \leq 0.15$ mentioned in Sect. 3.2 becomes active at this point and leads to abrupt venting of the brake cylinder; (iii) a certain level of chattering often comes along when using sliding mode control. Anyhow, a reasonable braking behavior at low v_x and low μ_0 is a critical situation for every control approach. In the end, the significant reduction of braking distances with ABC confirms the great potential of this adhesion-based control concept.

5 Conclusions and Outlook

The present work introduces a novel adhesion-based brake control (ABC) concept. This concept combines the adhesion signal provided by a generic and numerically efficient Kalman filter with the slip information to reach the maximal adhesion and, in consequence, to minimize the braking distance under bad and especially changing wheel-rail conditions. The potential of this concept is validated in numeric simulations of three challenging test scenarios. The reductions of braking distances reach from 8.8% to 12.9% compared to a simple slip-based brake control.

As a next step, ABC will be integrated into the real-time test rig environment *NGT FuN* [7] at the Institute of System Dynamics and Control, for a Hardware-in-the-Loop verification of the control concept. Since *NGT FuN* operates under a strict power and speed limitation, a test campaign for the validation of the entire performance of ABC will be planned on external test rigs.

References

1. Rail Accident Investigation Branch: Station overrun incident at Stonegate, East Sussex, 8 November 2010. https://www.gov.uk/raib-reports/station-overrun-incident-at-stonegate-east-sussex. Accessed 05 July 2021

2. Stützle, T., Engelhardt, T., Enning, M., Abel, D.: Wheelslide and wheelskid protection for a single-wheel drive and brake module (SDBM) for rail vehicles. IFAC Proc. Vol. **41**(2), 3606–3611 (2008)
3. Lee, N.-J., Kang, C.-G.: Wheel slide protection control using a command map and Smith predictor for the pneumatic brake system of a railway vehicle. Veh. Syst. Dyn. **54**(10), 1491–1510 (2016)
4. Yamashita, M., Soeda T.: Anti-slip re-adhesion control method for increasing the tractive force of locomotives through the early detection of wheel slip convergence. In: European Conference on Power Electronics and Applications, Geneva, Switzerland, pp. 1–10 (2015)
5. Mayer, R., Rasel, T.: Höhere Zugtaktung: Neuartiger Gleitschutz für eine verbesserte Auslastung der Schieneninfrastruktur. ZEVrail **144**(11–12), 438–442 (2020)
6. Zirek, A., Onat, A.: A novel anti-slip control approach for railway vehicles with traction based on adhesion estimation with swarm intelligence. Railway Eng. Sci. **28**(4), 346–364 (2020). https://doi.org/10.1007/s40534-020-00223-w
7. Lüdicke, D., Krüger, D., Weber, C., Goetjes, B., Heckmann, A.: DLR Forschungsinfrastruktur NGT-Fahrwerk (NGT-FuN). ETR - Eisenbahntechnische Rundschau DVV Media Group **70**(3), 62–68 (2021)
8. Modelica Association: Modelica. https://modelica.org/. Accessed 05 July 2021
9. Modelica Association: FMI standard. https://fmi-standard.org/. Accessed 05 July 2021
10. Schwarz, C., Lüdicke, D., Heckmann, B.: Friction estimation for railway brake systems in field tests. In: International Railway Symposium Aachen, pp. 608–623 (2019)
11. Ehret, M.: Identification of a dynamic friction model for railway disc brakes. Proc. Inst. Mech. Eng. F J. Rail Rapid Transit **235**(10), 1214–1224 (2021)
12. Polach, O.: Creep forces in simulations of traction vehicles running on adhesion limit. Wear **258**(7–8), 992–1000 (2005)
13. Shrestha, S., Spiryagin, M., Wu, Q.: Friction condition characterization for rail vehicle advanced braking system. Mech. Syst. Signal Process. **134**, 106324 (2019)
14. Schwarz, C., Keck, A.: Simultaneous estimation of wheel-rail adhesion and brake friction behaviour. IFAC-PapersOnLine **53**(2), 8470–8475 (2020)
15. Schwarz, C., Brembeck, J., Heckmann, B.: Dynamics observer for the longitudinal behavior of a wheelset on a roller rig. Proc. Inst. Mech. Eng. F J. Rail Rapid Transit **233**(10), 1112–1119 (2019)
16. The Commission of the European Communities: Comission Decision of 21 February 2008 concerning a technical specification for interoperability (TSI) relating to the rolling stock sub-system of the trans-European high-speed rail system. In: Official Journal of the European Union, March 2008
17. Utkin, V.: Sliding mode control design principles and applications to electric drives. IEEE Trans. Industr. Electron. **40**(1), 23–36 (1993)